Efficient SOM-Based ATR Method for SAR Imagery With Azimuth Angular Variations

Shouhei Ohno, Shouhei Kidera, *Member, IEEE*, and Tetsuo Kirimoto, *Senior Member, IEEE*

***Abstract*—The microwave imaging technique, especially for synthetic aperture radar (SAR), has significant advantages in providing high-resolution complex target images, even in darkness or adverse weather conditions. Nevertheless, it is still difficult for human operators to identify targets on SAR images because they are generated using radio signals with wavelengths at the order of cm. To deal with this, various approaches for efficient automatic target recognition (ATR), based on neural networks or support vector machines (SVM), have been developed. Previously we proposed a promising ATR method using a supervised self-organizing map (SOM), where a binarized SAR image is accurately classified by exploiting the unified distance matrix (U-matrix) metric. Although this method enhances ATR performance considerably, even with SAR images heavily contaminated by random noise, the calculation burden is enormous under expansions of scale and then cannot maintain the ATR performance, especially in cases with azimuth angle variations. In this letter, we propose a constrained learning scheme for generating the SOM and introduce the A-star algorithm to handle SOM scale expansion. Experimental investigations demonstrate the effectiveness of our proposed method.**

***Index Terms*—Automatic target recognition (ATR), fast algorithm, supervised self organizing map, synthetic aperture radar (SAR) imagery.**

I. Introduction

MICROWAVE imaging is one of the most useful tools for weather-impervious measurement of terrain or sea surfaces. As an indispensable imaging methodology, synthetic aperture radar (SAR) has been massively expanded to a wide variety of environmental sensing issues, such as afflicted-area assessments or coastal security for the identification of unidentified ships or airplanes. Since the spatial resolution of SAR is relatively inferior to that of optical sensor, it is still difficult for an inexperienced operator to recognize targets in SAR images compared with optically acquired images, because SAR images are generated by radio signals with wavelengths at the order of cm.

To realize automatic target recognition (ATR), various type of methods have been developed in recent decades. These include machine learning approaches, such as neural networks [1] and support vector machines (SVM) [2], where polarimetric data or range-profile feature are efficiently exploited to enhance the ATR performance [3]. Moreover, methods based on self-organizing maps (SOMs) heve been developed to detect floods or ships with SAR imagery [4], [5]. In particular, there are many reports stating that neural-network-based classification retains a certain level of accuracy in target recognition. However, these approaches result in seriously degraded classification accuracy when the available SAR images are highly contaminated by random noise. This is because classification by these approaches relies mainly on assessing the differences in output obtained from test and training inputs.

To enhance detection performance, we previously proposed an ATR method using supervised SOM and U-matrix metrics [6]. This method first generates a SOM using reliable SAR images as training data, where the batch learning (BL) approach [7] and torus SOM [8] are adopted in the learning process to obtain a consistent clustering result. In the classification process for this method, the U-matrix potential field generated by the final SOM is appropriately assessed using a path integral formulation. The literature [9] has already demonstrated that this method remarkably enhances ATR performance compared with that obtained by major neural-network-based approaches. However, because the method assesses the U-matrix metric by fully searching its potential field, the node scale corresponding to the SOM is critically limited owing to the exponential growth of the calculation. Thus, it is not suitable for ATR issues requiring a greater large-scale SOM.

To overcome this difficulty, this letter presents a revision of the earlier method [9], using an A-star algorithm [10] to calculate the U-matrix metric as a faster means of assessing the U-matrix field. For more robust classification, we also introduce a constrained training process, where each training node for the same target, but with different azimuth angles, are proximately located on the SOM. Finally, using experimental data obtained from 1/100 scaled-down models of the X-band radar system, it is demonstrated that the proposed ATR method successfully classifies SAR images, even under large angular variations with noisy cases.

II. System Model

Fig. 1 shows the geometry of the observation model assumed in this study. It assumes a mono-static radar, where a set of transmitting and receiving antenna is scanned along the straight line as $y = y_0$, $z = z_0$. The location of a target is set at $z = 0$, the off-nadir angle is θ, the azimuth angle is ϕ. Each antenna receives the reflection signals $s(x, f)$ at each frequency f. The SAR complex image focused on the $z = 0$ plane is defined as $I(x, y)$. The SAR image is binarized as

$$I^{\mathrm{bi}}(x,y) = \begin{cases} 1 & (\|I(x,y)\| \geq I_{\mathrm{th}}) \\ 0 & (\text{otherwise}) \end{cases} \tag{1}$$

Manuscript received October 3, 2013; revised February 2, 2014 and March 13, 2014; accepted March 17, 2014. Date of publication April 22, 2014; date of current version May 22, 2014.

The authors are with the Graduate School of Informatics and Engineering, The University of Electro-Communications, Tokyo 182-0021, Japan (e-mail: oono@secure.ee.uec.ac.jp).

Color versions of one or more of the figures in this paper are available online at http://ieeexplore.ieee.org.

Digital Object Identifier 10.1109/LGRS.2014.2313626

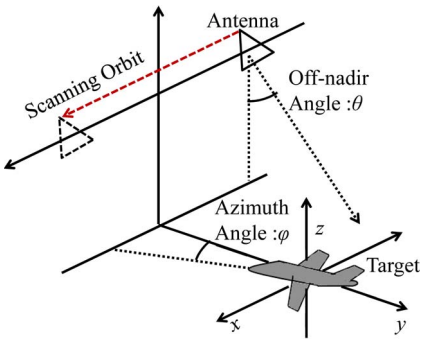

Fig. 1. Observation geometry and system model.

where the binarization threshold $I_{\rm th}$ is determined by Otsu's discriminant analysis method [11]. In this method, optimal threshold $I_{\rm th}$ is determined automatically from the interclass and intraclass variances, the latter having an advantage of being independent of outliers.

III. Conventional Method

This section briefly describes the principle and methodology of the conventional ATR method, as comparison to the proposed method. As commented in Section I, the method [9] is based on the supervised SOM and U-matrix metric [6]; in the training stage, the SOM is preliminary generated using reliable SAR images as training data. Here, "reliable image" indicates an image with a sufficiently high SNR. The SOM map consists of $M_X \times M_Y$ nodes (neurons). The training binarized SAR images are set as $\boldsymbol{x} = [I^{\rm bi}(x_1, y_1), \ldots, I^{\rm bi}(x_1, y_{N_y-1}), I^{\rm bi}(x_2, y_1), \ldots, I^{\rm bi}(x_2, y_{N_y-1}), \ldots, I^{\rm bi}(x_{N_x-1}, y_1), \ldots, I^{\rm bi}(x_{N_x-1}, y_{N_y-1})]$ to represent the whole SAR image after binarization. The training binarized SAR images are defined as $\boldsymbol{x}_k^{\rm tr}, (k=1, 2, \ldots, N_{\rm tr})$. The location of each node is denoted by $\boldsymbol{p}$, and the node has an output image defined as $\boldsymbol{y}(\boldsymbol{p}; t)$, where t is the number of training trials. As a simpler, yet similar process to principal component analysis (PCA), an initial output for each node is defined using a linear mixture of the training images as

$$\boldsymbol{y}(\boldsymbol{p}; 1) = \frac{\sum_{k=1}^{N_{\rm tr}} a_k(\boldsymbol{p}) \boldsymbol{x}_k^{\rm tr}}{\sum_{k=1}^{N_{\rm tr}} a_k(\boldsymbol{p})} \tag{2}$$

where $a_k(\boldsymbol{p})$ is a uniform random numbers for [0,1] with variant of $\boldsymbol{p}$. Next, for the kth training data $\boldsymbol{x}_k^{\rm tr} (k = 1, 2, \ldots, N_{\rm tr})$, the location of the winner node $\boldsymbol{p}_k(t)$ is determined to find where the Euclidean norm between training image $\boldsymbol{x}_k^{\rm tr}$ and the output $\boldsymbol{y}(\boldsymbol{p}; t)$ for each node becomes a minimum. After calculating $\boldsymbol{p}_k(t)$ for all the training data, the output of each node is updated by

$$\boldsymbol{y}(\boldsymbol{p}; t+1) = \boldsymbol{y}(\boldsymbol{p}; t) + \beta(t) \frac{\sum_{k=1}^{N_{\rm tr}} h\left(\hat{\boldsymbol{p}}_k(t), \boldsymbol{p}\right) \left(\boldsymbol{x}_k^{\rm tr} - \boldsymbol{y}(\boldsymbol{p}; t)\right)}{\sum_{k=1}^{N_{\rm tr}} h\left(\hat{\boldsymbol{p}}_k(t), \boldsymbol{p}\right)} \tag{3}$$

where $h(\hat{\boldsymbol{p}}_k(t), \boldsymbol{p})$ is the neighboring function as

$$h\left(\hat{\boldsymbol{p}}_k(t), \boldsymbol{p}\right) \times = \exp\left(-\frac{\|\hat{\boldsymbol{p}}_k(t) - \boldsymbol{p}\|}{2\sigma(t)^2}\right). \tag{4}$$

Here, t is training trials $(t = 1, 2, \ldots, T_{\rm som})$, $T_{\rm som}$ denotes the total number of training trials, $\beta(t)$ and $\sigma(t)$ are monotonically decreasing functions for t. The batch learning (BL) approach [7] is introduced so that the obtained SOM should be robust against the order of the training data sequence. Furthermore, to assess the entire region of the SOM under a fair standard, the periodical structure of SOM is considered as in [8]; these are classified as torus-type SOMs. Finally, the U-matrix potential field is generated by final SOM [6].

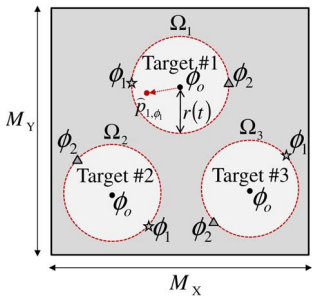

Fig. 2. Constrained learning on SOM.

In the classification stage, this method employs topological and U-matrix features of SOM, namely, for unknown image $\boldsymbol{x}$, the following metric is assessed:

$$R_k^{\rm som} = \min_{C(\boldsymbol{x}_k^{\rm tr}, \boldsymbol{x})} \int_{C(\boldsymbol{x}_k^{\rm tr}, \boldsymbol{x})} U(\boldsymbol{p}) {\rm d}\boldsymbol{p} \tag{5}$$

where $\boldsymbol{p}$ denotes the position of the U-matrix field and $C(\boldsymbol{x}_k^{\rm tr}, \boldsymbol{x})$ denotes all possible paths from $\hat{\boldsymbol{p}}_k(T_{\rm som})$ to $\hat{\boldsymbol{p}}$ for Manhattan distance. Here, the path integral of (5) should be discretized to reduce the computation burden as in [9]. $U(\boldsymbol{p})$ is the U-matrix value on $\boldsymbol{p}$, $\hat{\boldsymbol{p}}_k(T_{\rm som})$ expresses each winner node for the kth training data and $\hat{\boldsymbol{p}}(\boldsymbol{x})$ is the winner node of the unknown input, which is determined in the same way as learning process. While this method suitably assesses the U-matrix potential and achieves a more accurate classification, the node scale of a SOM is critically limited because of exponential growth in the calculation. Thus, it is not suitable for various ATR cases requiring a more large-scale SOM.

IV. Proposed Method

To overcome this problem, this letter significantly revises the previous method [9] by introducing an efficient learning and classifying scheme as follows.

A. Node Constrained SOM Generation

In the learning phase, a node constrained training scheme is introduced to improve the robustness against variation in observation angles, where the winner node locations for the same type target but different observation angles should be adjoined on the SOM. Fig. 2 shows the node constrained learning scheme. In the initialization of the SOM, each winner node for training data with the observation angle ϕ_0 is determined so that the Euclidean distance among those nodes maintains the same distance level. Then, in the next step, the winner-node determination of each target with different observation angles ϕ_i is constrained as

$$\hat{\boldsymbol{p}}_{k,\phi_i}(t) = \arg\min_{\boldsymbol{p} \in \Omega_k} \left\| \boldsymbol{y}(\boldsymbol{p}; t) - \boldsymbol{x}_{k,\phi_i}^{\rm tr} \right\| \tag{6}$$

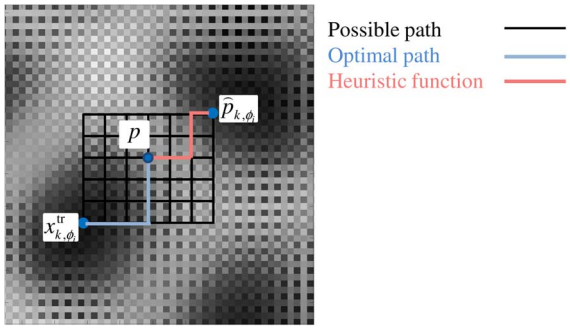

Fig. 3. Relationship among optimal path and heuristic function.

where Ω_k denotes the inner area of the circle with center $\hat{\boldsymbol{p}}_{k,\phi_0}$ and the radius $r(t)$ is a monotonically increasing function in the trial number t.

B. Acceleration for Classification Process With A-Star Algorithm

In the classification stage, we also introduce the A-star algorithm [10] in calculating the integral of the U-matrix field in (5). With this algorithm, the minimum U-matrix cost between two nodes is calculated by sequentially updating an optimal path and reducing the redundant evaluation for the path, that does not pass through the present optimal path. To start searching from the path which is expected to be more optimal, the heuristic function $h^*(\boldsymbol{p})$ that indicates the predicted value to the goal is determined as

$$h^*(\boldsymbol{p}) \leq h(\boldsymbol{p}) \tag{7}$$

where $h(\boldsymbol{p})$ denotes the actual minimum cost between the present node $\boldsymbol{p}$ and the goal. In the proposed method, $h^*(\boldsymbol{p})$ is set to the product between the minimum value of U-matrix field and the Manhattan distance between the present node $\boldsymbol{p}$ and the goal to satisfy the condition in (7). Fig. 3 shows an optimal path calculated by the A-star algorithm on the U-matrix field.

C. Procedure of the Proposed Method

Fig. 4 outlines the actual procedures in the proposed method, which is summarized as follows.

- Step 1) Initial images for all nodes are defined using a linear mixture of the training images.
- Step 2) For the kth training data, the locations of the winner node denote as $\hat{\boldsymbol{p}}_{k,\phi_0}(t)$ and $\hat{\boldsymbol{p}}_{k,\phi_i}(t)$ are determined using (6), where $\hat{\boldsymbol{p}}_{k,\phi_i}(t)$ should be adjacent to $\hat{\boldsymbol{p}}_{k,\phi_0}(t)$. (Constrained learning process)
- Step 3) After calculating $\hat{\boldsymbol{p}}_{k,\phi_0}(t)$ and $\hat{\boldsymbol{p}}_{k,\phi_i}(t)$ for all the training data, the output of each node is updated using (3). (Batch learning process)
- Step 4) Step 2) to Step 3) are repeated until the trial number reaches T_{som}.
- Step 5) U-matrix potential field is generated by the final SOM.
- Step 6) For unknown data $\boldsymbol{x}$, an appropriate target class is determined by evaluating (5), where the A-star algorithm is used to accelerate the calculation.

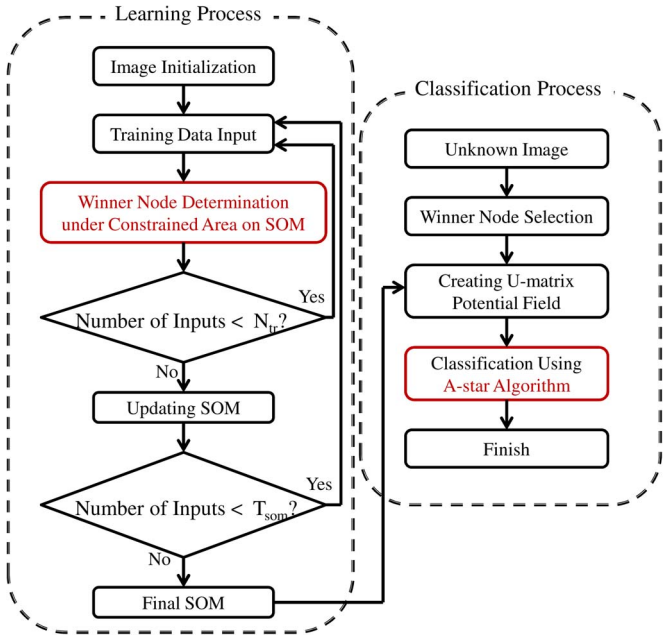

Fig. 4. Flowchart of the proposed method.

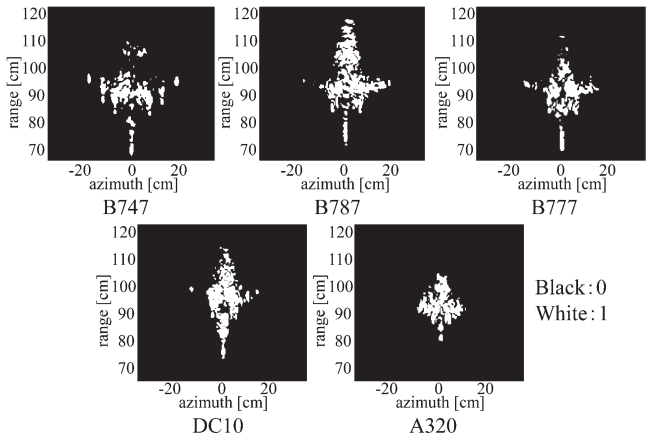

Fig. 5. Binarized images for each airplane at $\phi = 0°$.

V. Performance Evaluation With Experimental Data

This section describes the ATR performance evaluations for each method using experimental data. A 1/100-scale model of the X-band radar system, except for the center frequency, is assumed. Here, the off-nadir angle θ is 54.7°, the height of antenna is 1.154 m, the frequency is swept from 24 to 40 GHz, and the aperture length is 1.6 m. The observation azimuth angle ϕ is $-30° \leq \phi \leq 30°$ with 1° interval. Figs. 5 and 6 show binarized SAR images for azimuth angle $\phi = 0°$ and $\phi = -20°$ of five types of airplanes, B747, B787, B777, DC10, and A320, respectively. As shown in these figures, the SAR image with different azimuth angles are hardly compensated by the image rotation, which makes this issue more difficult. In addition, in this case, speckle noise is adequately removed by the binarization process. The training data for each aircraft with $\phi_0 = 0°$ and $\phi_1 = -20°$, $\phi_2 = 20°$ are used for generating the SOM. In this experiment, a reliable image for the training data can be obtained if a 20 dB amplifier is used on the transmitting side.

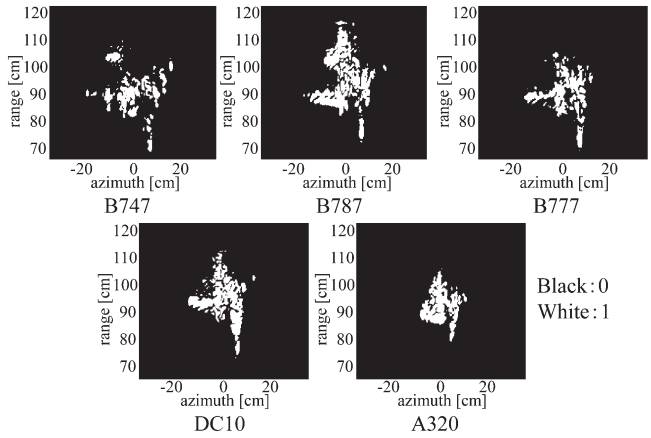

Fig. 6. Binarized images for each airplane at $\phi = -20°$.

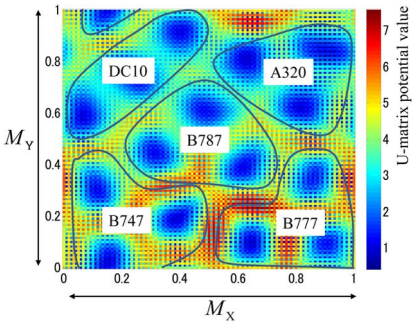

Fig. 7. U-matrix potential field created by the proposed method.

In addition, the center location of each SAR image is adjusted through cross-correlation with the training SAR image.

Under the limitation of the computational resource, the SOM size in the conventional method is set to 26×26 as described hereinbelow. The proposed method can expand the SOM size by significantly reducing the computational load using A-star algorithm. Generally, the greater is the number of SOM nodes used, the more training patterns can be dealt with. However, a larger SOM scale results in greater calculation burden in generating the SOM and classifying the patterns using the SOM's U-matrix. As a tradeoff, we use 61×61 nodes for the SOM. In both methods, the 15 training data for the five target types with three different observation angles were used in generating the SOM. Fig. 7 shows the U-matrix field generated by the proposed method, where the total number of training trials is $T_{\mathrm{som}} = 50$. In addition, the winner node of the same aircraft but different observation angles is adjoined because of the node constrained learning process. This characteristic contributes to enhance the accuracy for target recognition and robustness against observation-angle variations.

A. Comparison of Calculation Amount in Classification Process

This subsection investigates the calculation burden for each method in the classification phase using the U-matrix metric. Fig. 8 shows the required calculation amount $C_N(N_{\mathrm{X}}, N_Y)$ versus the number of nodes, assuming the situation mentioned in the previous subsection, where the number of nodes is expressed as $N_{\mathrm{X}} = N_{\mathrm{Y}}$. $C_N(N_{\mathrm{X}}, N_Y)$ denotes the required number of paths between the start and goal in evaluating (5).

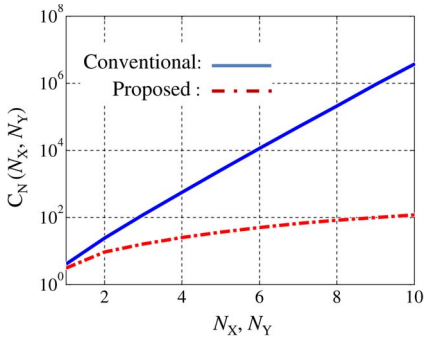

Fig. 8. Calculation Amount of each Searching Method.

TABLE I
COMPARISON OF PROBABILITY FOR CORRECT CLASSIFICATION AT SNR = 40 dB

	B747	B787	B777	DC10	A320
SVM[%]	100	100	96	93	98
SOM(Conventional) [%]	92	80	55	78	100
SOM(Proposed) [%]	100	100	93	98	98

This figure clearly indicates that the calculation amount of the conventional approach increases exponentially with the node size. In contrast, the A-star algorithm used in the proposed method significantly suppresses the exponential increase in calculation amount with node size. This is because the A-star algorithm sequentially removes a redundant paths in minimizing the evaluation function in (4) by considering a provisional optimal path, which is assessed using a heuristic function.

B. Performance Evaluation for ATR

Next, we discuss the robustness for angular variations or random noise of each method. Table I shows the classification results as the probability of correct classification for each azimuth angle of the five airplane types. In this case, the mean signal-noise ratio (SNR) is 40 dB, where SNR is defined as the ratio of the average power of the target area to that of the non-target area in the SAR image. These results demonstrate that while the conventional method fails to recognize the correct target in some cases, the proposed method is significantly more robust with respect to azimuth angle variation. This is because our proposed method readily expands the size of the SOM, where the same type of target with different azimuth angles is efficiently located on the SOM according to the procedure for node constrained training described in Section IV-A.

Additionally, we investigate ATR performance in lower SNR situations. In the case of simulating the receiver noise, additive Gaussian noise is numerically added to each unknown SAR image. Fig. 9 shows the binarized SAR images, numerically contaminated by random noise, with the SNR set to 18 dB. Table II shows probability of correct classification for each azimuth angle when the contaminated SAR images given in Fig. 9 are input into the final SOM as unknown images. Therefore, these results indicate that the proposed method has a considerably higher probability of correct classification than the conventional method even in noisier situations.

As additional discussions, although we adopt the binarized SAR image as the image feature in this study, we also tested other image features, such as complex-values or absolute values

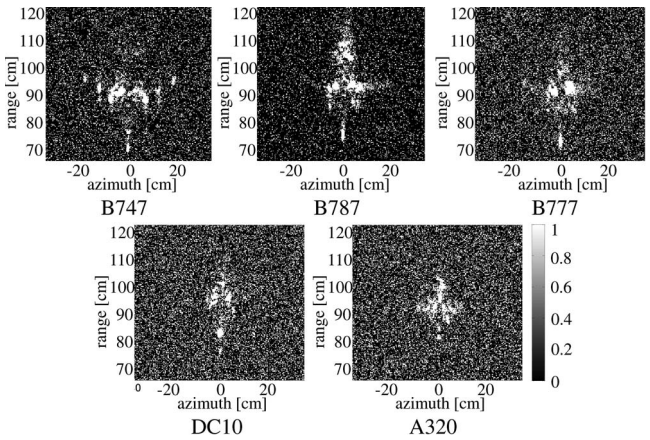

Fig. 9. Binarized images for each airplane at SNR $= 18$ dB.

TABLE II
COMPARISON OF PROBABILITY FOR CORRECT CLASSIFICATION AT SNR $= 18$ dB

	B747	B787	B777	DC10	A320
SVM[%]	95	98	50	88	0
SOM(Conventional) [%]	85	50	50	48	87
SOM(Proposed) [%]	90	66	67	92	95

TABLE III
COMPARISON OF PROBABILITY FOR CORRECT CLASSIFICATION IN DIFFERENCE THRESHOLD $I_{\rm th}$

	B747	B787	B777	DC10	A320
$I_{\rm th} \times 0.9$	100	93	80	97	98
$I_{\rm th} \times 1.0$	100	100	93	98	98
$I_{\rm th} \times 1.1$	100	97	85	97	95

of SAR images. In these cases, we confirmed that their robustness to angular variations degraded compared with the results obtained using binarized SAR inputs. This indicates that the absolute or phase information of SAR images is more sensitive to angular variations, and binarized input is more suitable for upgrading robustness. We also investigate sensitivity of the proposed method woth regard to the binarizing threshold. Table III shows the classification results when varying this threshold at SNR $= 40$ dB. The results indicate that the classification performance of the proposed method is not significantly changed as to the binarizing threshold. Note that, we assume only the receiver noise in this investigation. This is because an appropriate design of speckle noise is more complicated for this artificial target type, which is different from that of a volume scatter such as forest modeled in [12].

C. Comparison With SVM-Based Approaches

For comparison with the proposed method, this section introduces the conventional method using an SVM [13]. We adopt the LIBSVM tool [14] to support multiclass classification, using a soft margin SVM with a radial basis function as the kernel function. Similar to the other methods, the inputs for the SVM are binarized SAR images $\boldsymbol{x}_k^{\rm tr}$, $(k = 1, 2, \ldots, N_{\rm tr})$, with the azimuth angles set to $\phi_0 = 0^\circ$, $\phi_1 = -20^\circ$ and $\phi_2 = 20^\circ$. As shown in the Table I with SNR $= 40$ dB, the SVM approach provides almost the same accuracy as the proposed method. However, with lower SNR as shown in Table II, the classification accuracy by the SVM-based method degrades significantly compared with the proposed method, especially for B777 and A320. This result also verify the effectiveness of the proposed method.

VI. CONCLUSION

This letter proposed a novel ATR method for SAR imagery with supervised SOM, where the A-star algorithm is introduced to deal with a larger-scale SOM and the node constrained learning process is implemented to enhance the robustness against observation-angle variations. The experimental validations assuming a typical X-band radar system verified that our revised method remarkably upgrades the ATR performance in terms of accuracy and robustness under angular variations or lower SNR situations. A disadvantage of the proposed method is that the calculation time is significantly greater than that required by neural network or SVM-based approaches. Moreover, the acceleration of the classification process is important for practical use.

As a final remark, since we cannot find an appropriate data set comprising real observations, that is, images representing angular variations of the same target, this letter only considered experimental results obtained assuming the 1/100 scale model of X-band radar. For real data, we need to consider the dependency of sensor-orbit for correct classification. Extending the proposed method to full polarimetric data would be interesting to improve classification performance.

REFERENCES

[1] B. Widrow, R. G. Winter, and R. A. Baxter, "Layered neural nets for pattern recognition," *IEEE Trans. Acoust., Speech Signal Process.*, vol. 36, no. 7, pp. 1109–1118, Jul. 1988.
[2] X. Yu, Y. Li, and L. C. Jiao, "SAR automatic target recognition based on classifies fusion," in *Proc. Int. Workshop Multi-Platform Multi-Sensor Remote Sens. Mapping*, Jan. 2011, pp. 1–5.
[3] C. M. Pilcher and A. Khotanzad, "Maritime ATR using classifier combination and high resolution range profiles," *IEEE Trans. Aerosp. Electron. Syst.*, vol. 47, no. 4, pp. 2558–2573, Oct. 2011.
[4] S. Skakun, "A neural network approach to flood mapping using satellite imagery," *Comput. Informat.*, vol. 29, no. 6, pp. 1013–1024, 2010.
[5] D. Howard, S. C. Roberts, and R. Brankin, "Evolution of ship detectors for satellite SAR imagery," in *In Genetic Programming*. New York, NY, USA: Springer-Verlag, 1999, pp. 135–148.
[6] A. Ultsch and H. P. Siemon, "Kohonen's self organizing feature maps for exploratory data analysis," in *Proc. Int. Neural Netw. Conf.*, 1990, pp. 305–308.
[7] H. Matsushita and Y. Nishio, "Batch-learning self-organization map with false-neighbour degree between neurons," in *Proc. IEEE IJCNN*, Jun. 2008, pp. 2259–2266.
[8] M. Ito, T. Miyoshi, and H. Masuyama, "The characteristics of the torus self organizing map," in *Proc. 6th Int. Conf. Soft Comput.*, Fukuoka, Japan, 2000, pp. 239–244.
[9] S. Kidera and T. Kirimoto, "Accurate and robust automatic target recognition method for SAR imagery with SOM-based classification," *IEICE Trans. Commun.*, vol. E95-B, no. 11, pp. 3563–3571, Nov. 2012.
[10] E. P. Hart, N. J. Nilsson, and B. Raphael, "A formal basis for the heuristic determination of minimum cost paths," *IEEE Trans. Syst. Sci. Cybern.*, vol. SSC-4, no. 2, pp. 100–107, Jul. 1968.
[11] N. Otsu, "A threshold selection method from gray-level histograms," *IEEE Trans. Syst., Man Cybern.*, vol. SSC-9, no. 1, pp. 62–66, Jan. 1979.
[12] R. Bolter, M. Gelautz, and F. Leberl, "SAR speckle simulation," in *Proc. Int. Archives Photogramm. Remote Sens.*, 1996, vol. 31, pp. 20–25.
[13] C. Cortes and V. Vapnik, "Support vector networks," *Mach. Learn.*, vol. 20, no. 3, pp. 273–297, Sep. 1995.
[14] C. C. Chang and C. J. Lin, "LIBSVM: A Library for Support Vector Machines, C. Cortes and V. Vapnik, Support vector networks," *ACM Trans. Intell. Syst. Technol.*, vol. 2, no. 3, p. 27, Apr. 2011. [Online]. Available: http://www.csie.ntu.edu.tw/~cjlin/libsvm/